

Resolving *Trypanosoma brucei* Flagellar Structure by Cryo-Electron Tomography

Jennifer Dai^{1,a}

¹Fudan University, Biological Sciences Department, 220 Handan Rd., Yangpu District, Shanghai, China

Abstract. *Trypanosoma brucei* is a unicellular eukaryote that can cause human African trypanosomiasis, which has continued to evolve and spread. The key feature of these parasites is that they have a flagellum consists of a typical 9 + 2 axoneme and a lattice-like paraflagellar rod (PFR). It attached to the cell body and is responsible for cell motility, cytokinesis, and morphogenesis. The present study demonstrates the detailed structure and defines the length of the axoneme and three domains of the paraflagellar rod (PFR) using cryo-electron tomography of *Trypanosoma brucei* flagella. The performed analysis revealed the double-headed structure of the outer-arm dynein, the internal structure of PFR and identified repeating structure in the flagella. Since these structures are critical to the pathogenicity of *Trypanosoma brucei*, and understanding their organization would help in finding treatments against African trypanosomiasis.

1 Introduction

Trypanosoma brucei is a unicellular eukaryote that contributes to numerous diseases such as human African trypanosomiasis (HAT) [1]. It is also known as African sleeping sickness which occurs in humans as well as Nagana in cattle. This disease has infected large numbers of humans in 36 countries of sub-Saharan Africa, with an estimated actual number of cases of about 10,000 and an estimated 65 million people at risk [2].

HAT is spread through the bite of infected tsetse fly (*Glossina*) [3]. This parasite has developed a complex life cycle with different progressive stages, which has assisted proliferation in mammalian hosts. Initially, trypanosomes propagate in subcutaneous tissue, blood, and lymph. The parasite subsequently crosses the blood-brain barrier and infects the central nervous system [4,5]. The duration of the entire process takes several years for *Trypanosoma* [1,2].

The first stage of the disease is called hemolymph, which is accompanied by fever, headache, arthralgia, and itching (pruritus). The second stage, called the neural stage, is the period when the parasite begins to cross the blood-brain barrier and invade the host's central nervous system. In general, the disease begins to exhibit the following signs and symptoms: delirium, sensory disturbance, and ataxia. Disturbance of the sleep cycle is a major feature of HAT's second stage [6,7]. Without treatment, sleeping sickness can be fatal. However, we currently don't have effective vaccines for disease treatment and there are also problems with toxicity and resistance to drugs on the market to treat these diseases [8].

The most characteristic feature of trypanosomes is the presence of a single flagellum that is highly

conserved in numerous types of cells (Fig1). The basic unit responsible for the motion of the flagellum is the axoneme, which acts as a cytoskeletal motor. Axoneme consists of microtubules, dyneins, and auxiliary protein complexes [9]. It plays a vital role in multiple aspects of *T. brucei* biology, such as cell movement, virulence in the mammalian host, transmission, and host-parasite interactions [10]. Therefore, understanding the structure and function of the flagellum is crucial in the fight against its pathogenicity.

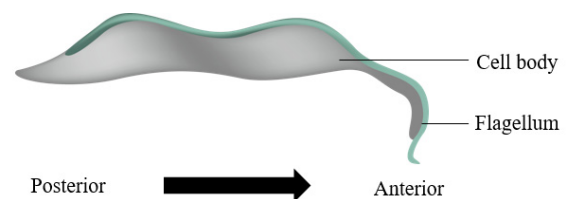


Figure 1. Overview of the *Trypanosoma brucei*.

The image was generated with the Adobe Photoshop software. *T. brucei* attaches itself to a portion of the flagellum, proceeds by whipping the free end of the flagellum back and forth. Counter-intuitively, the resulting direction of motion is the tail of the flagella. Trypanosomes' unusual use of flagella suggests that the internal structure of the flagella is equally unusual, an extension of the principle that structure and function are closely related in biomechanics.

Cryo-electron tomography (Cryo-ET) is a convenient tool used to study the structure of *T. brucei*, since the combination of tomography with tilting of the sample allows generating a three-dimensional (3-D) reconstruction of the specimens, and provides a spatial resolution of the organism structures of approximately 5

^a Corresponding author: jenniferxddai@yeah.net

nm. In comparison with single-particle analysis, tomography offers a clearer understanding of the orientation of samples, because individual particles randomly distributed on the grid can have different spatial orientation that cannot be deduced from a two-dimensional image. Therefore, the necessary information about the orientation of samples can be obtained by slanting samples, which simplifies the back-projection calculation. In the experiment shown, all the data were processed by eTomo software [11], which allows multiple images to be stitched together using 5 nm gold nanoparticles as reference points. In tomography, images are taken at increments of -2° , from -60° to $+60^\circ$, to generate a total of 61 images.

In this experiment, back-projection and Simultaneous Iterative Reconstruction Technique (SIRT) algorithms were employed to obtain a 3-D reconstruction of the samples. SIRT utilizes the density of electrons along the projection line to make a raw estimate of the projected tomographic image. For each pixel, the difference between the original projection and the re-projection is calculated and used as the error of the original estimate. By distributing this difference between each pixel along its contribution ray, all errors of the tomographic image are added substantially by the back-projection algorithm. The use of SIRT requires finding the number of iterations that yields fully visible fine detail while maintaining the noise below the value of the back-projection signal [12].

The axoneme of *T. brucei* has been previously demonstrated to consist of periodic repeating units, approximately 96 nm in length. Each unit has four subunits of outer-arm dynein, inner-arm dynein, nexin-dynein regulatory complex (NDRC) and three radial spokes that converge into the central pair of microtubules [13]. The present study analyzed the cross-section of flagella by cryo-ET and 3-D reconstruction. The average distance between each outer-arm dynein and between the center of each group of triplet radial spokes was calculated; thus, the repeat fragments of flagella were further determined that a 96 nm repeat contains four outer-arm dyneins and three radial spokes.

Recent studies have elucidated the internal structure of the axoneme and the three domains of PFR. It has been also demonstrated that PFR is associated with axoneme doublet microtubules and the domains of flagella attachment [14]. Thus far, the subunit composition of *T. brucei* axonemal dynein has not been determined, but it can be predicted that the external dynein is double-headed. The current work allowed the utilization of the axial view to determine the internal structure of each domain of PFR and identify the double-head structure of the outer-arm dynein.

The current work utilized the images and data sets collected by cryo-ET, and the data were visualized using eTomo [11]. The 3-D tomograms were instrumental in the exploration and analysis of the structure of the flagellum structure. The study was focused on the identification of the internal architecture of the axoneme and PFR, and revealed the double-head structure of axoneme dynein, and the reticular and wavy structure of PFR. Additionally, the distance between each dynein and

between each group of triple radial spokes was calculated to verify further the 96 nm repeat unit. The overarching goal was to screen crucial targets for the chemical prevention and therapy of African trypanosomiasis.

2 Materials and methods

2.1 Cryo-ET sample preparation and Data acquisition

We use flash-freezing to prepare the biology sample for cryo-ET. Our data were processed using the tomographic imaging program eTomo, which allows multiple images to be stitched together using 5nm gold nanoparticles as a reference point. In tomography, images are taken at increments of -2° from -60° to $+60^\circ$ to produce a total of 61 images. Each image was a cross section of the sample, then we use eTomo to align tomography tilt series files and then reconstruct them into a 3-D tomogram.

2.2 Data processing

Tomography data sets are reconstructed in 3-D image by the IMOD software package [11]. The version of the software used for this research was 4.9.5. To brief introduce, the series were analyzed by performing the following steps: removing X-rays section, creating a coarse-aligned stack, using patch tracking to create a fiducial model, aligning the serial tiles, and, finally, adjusting the reconstruction and creating a tomogram utilizing the algorithms of both back-projection and SIRT. We can search IMOD User's Guide for Version 4.9 for further information on how to reconstruct the tilt series [12].

2.3 Data analysis

First, the raw data of tilt series were analyzed before reconstruction by IMOD [11]. By observing the information contained in raw data from different angles, we identified the sections of the axoneme and PFR, and obtained preliminary measurements of these structures. Uncertain and ambiguous structures were highlighted for further analysis in the 3-D reconstructed images.

Subsequently, the analysis of data sets reconstructed by the back-projection algorithm and SIRT algorithm were performed. In the cross-section of *T. brucei*, the 9+2 structure of axoneme and the three domains of PFR were clearly identified. The diameters of outer doublet microtubules and central apparatus were measured and averaged to achieve greater accuracy. Moreover, the length and proportion of the three domains of PFR in cross-section were calculated. A comparison of the structures reconstructed by the back-projection and the SIRT algorithms revealed the presence of differences between the two protocols in terms of the completeness and sharpness of the reconstructed images. To display the 9+2 structure of axoneme more distinctly, Adobe

Photoshop software was used to generate images of the arrangement of microtubules in the flagellum of *T. brucei*.

Tilt series of the longitudinal view of *T. brucei* axoneme were re-analyzed from different angles to identify the optimal view visualizing the morphology of dynein. Schematic representations reflecting the morphology and structure of dynein were prepared to verify the double-head model of outer-arm dynein. The distance between each dynein at this angle was measured, and statistical chart was prepared to show the distribution and average distance between dynein molecules. Subsequently, the complete form of radial spoke was observed, the distance between each group of triple radial spokes was determined, and statistical data were plotted. Finally, the internal structure of PFR was analyzed in which three distinct domains and their internal structural features were identified.

3 Results

3.1 Longitudinal view of *T. brucei* axoneme presented by raw data

Fig2 contains images illustrating the internal structure of the flagellum, including regions of the axoneme and PFR. Inside the axoneme, the outer doublet of microtubules and the central pair apparatus are clearly visible along the flagellum. In the section of PFR, we can see the amorphous material and the tubular structure which lie furthest away from axoneme. Each tubule is approximately 22nm in diameter in this view. However, it is unclear if the PFR consist of tubular structures because of resolution is limited. Although the raw data allow identifying the partitions of the axoneme and the PFR, the structure of dynein inside the axoneme and the different partitions of PFR are not rendered clearly due to a large number of overlaps.

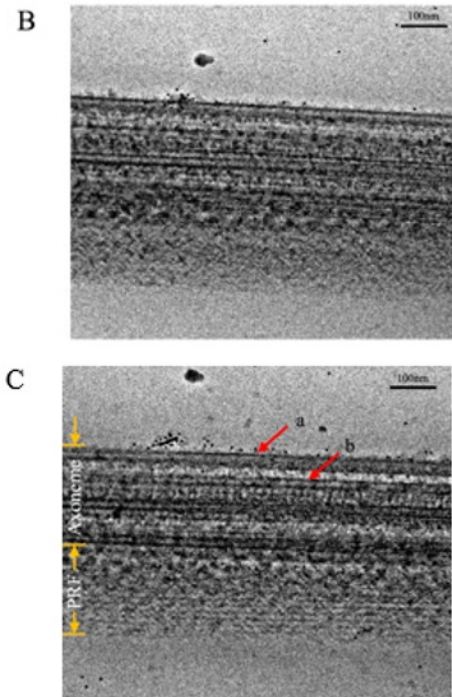
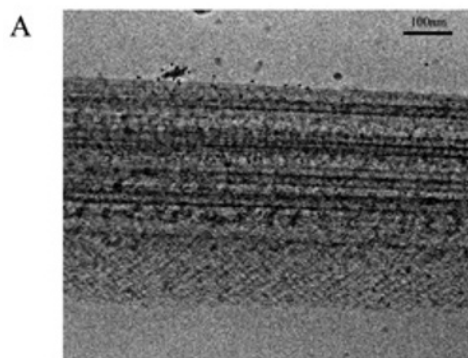


Figure 2. Longitudinal view of *T. brucei* axoneme.

These images are the raw data of tilt series of *T. brucei*.

(A) There are 61 images in the tilt series, and this image is the 31st.

(B) This image is the 47th of the tile series.

(C) This image is the 16th of the tile series. The labels in the diagram are shown below: a. outer doublet microtubules; b. central pair apparatus. Each tubule is approximately 22 nm in diameter.

3.2 Transection of *T. brucei* axoneme

Fig3 depicts nine outer doublet microtubules containing the A- and B-tubules. The central pair apparatus, surrounded by the central sheath, is present in the middle. The PFR is comprised of three domains: proximal, intermediate, and distal. This image (Fig3A) reveals also the structure of the axoneme, including outer doublet microtubules, outer-arm dyneins, inner-arm dyneins, NDRC, central pair apparatus and central sheath, documenting the 9 + 2 structure of the axoneme. Each microtubule is approximately 24.3 nm in diameter. The length of the axoneme section is approximately 243 nm, and the length of PFR is approximately 209 nm. In this view, the length of the proximal, intermediate, and distal domains of the PFR are, respectively, 96 nm, 36 nm, and 56 nm. The ratios of the lengths of these domains are approximately 5.0:1.9:2.8, respectively.

Here, we can see the structure of outer-arm dynein, inner-arm dynein, NDRC, and central sheath after processing by back-projection algorithm (Fig3A). This level of detail is absent in the images processed by SIRT algorithm (Fig3B), reflecting the differences in the clarity and completeness between the imagery generated by the two algorithms. The pictures processed by back-

projection algorithm are more complete, while the resolution of images processed by SIRT is superior.

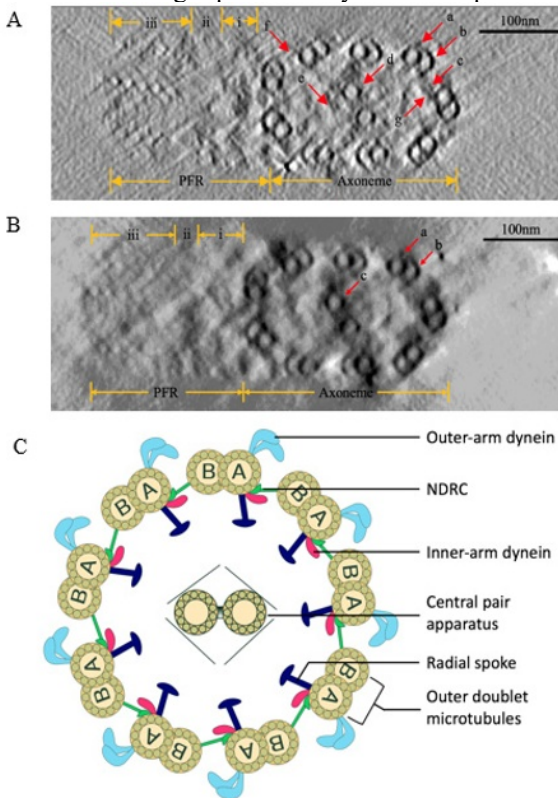


Figure 3.. Transection of *T. brucei* axoneme.

(A) Image generated by the back-projection algorithm with the IMOD software. The degree of x, y, z rotation is 0, and the view axis position is 269. The following labels are used in the diagram: a, A-tubule; b, B-tubule; c, NDRC; d, central pair apparatus; e, central sheath; f, outer-arm dynein; g, inner-arm dynein; i, proximal domain; ii, intermediate domain; iii, distal domain. The image reveals the structure of the axoneme, which includes outer double microtubules, outer-arm dyneins, inner-arm dyneins, NDRC, central pair apparatus and central sheath. The 9 + 2 structure of the axoneme is apparent.

(B) Image generated by the SIRT algorithm using the IMOD software. The degree of x, y, z rotation of this figure is 0, and view axis position is 293. The labels used in the diagram are as follows: a, A-tubule; b, B-tubule; c, central pair apparatus; i, proximal domain; ii, intermediate domain; iii, distal domain.

(C) Arrangement of microtubules in a flagellum of *T. brucei*. The image was generated with the Adobe Photoshop software.

The reconstruction of the tilt series allowed visualizing the internal structure of the axoneme and PFR. However, some information is missing, since biological samples are stored in vitreous ice, radiation will generate energy and high-energy electrons will bombard the samples and destroy them. Therefore, radiation damage was the main limitation of image acquisition, since it was necessary to obtain datasets at low radiation doses, restricting the total number of shots and tilt angles.

3.3 Longitudinal view of *T. brucei* axoneme

In Fig4(A), we show the internal structure of axoneme in longitudinal view of *T. brucei*, including outer-arm dyneins, inner-arm dyneins, central pair apparatus, and each microtubule is approximately 22.3 nm wide, and the width of the central pair apparatus is approximately 18.4 nm. Specially, we can resolve the structure of outer-arm dynein with high resolution in Fig4(B), which consists of two lobes of dynein with a thick head and a thin tail (Fig4D).

Here, we calculated the distance between each outer-arm dynein; a total of 43 data were collected (Fig4C). The distance between 23.3% of dyneins was from 21.79 to 23.10 nm, for 39.5% of dyneins the distance was from 23.10 to 24.39 nm, for 25.6% of dyneins the distance was from 24.39 to 25.69nm, and for 11.6% of dyneins the distance was from 25.69 nm to 26.99 nm. The average distance was 24.14nm, corresponding to the average length of the repeat unit of approximately 96.56 nm. These data verify that microtubules are arranged lengthwise in 96 nm repeats, as predicted by the model of the axoneme structure. However, given the limitation in the spatial resolution, the obtained value may be burdened by an error.

The distance between the center of each group of triple radial spokes shown in Fig3(E) was also measured. Thirteen groups of data were evaluated. The distance between 7.7% group of triple radial spokes ranges from 77.33 to 87.33 nm, the distance between 53.8% group of triple radial spokes ranges from 87.33 nm to 97.33 nm, and the distance between 38.5% group of triple radial spokes ranges from 97.33 nm to 107.33 nm (Fig4F). The average distance is 95.42 nm, a value close to the length of the 96 nm repeat unit.

Fig4(G) and Fig4(H) illustrate the three distinct domains of PFR. The proximal, intermediate, and distal domains are, respectively, 141.7, 25.9, and 35.4 nm in length. The ratios of the length of the proximal, intermediate, and distal domains are approximately 10:2:2.5. The image demonstrates that the proximal domain has a wavy structure, while the structure of the distal domain resembles a mesh (Fig 4G).

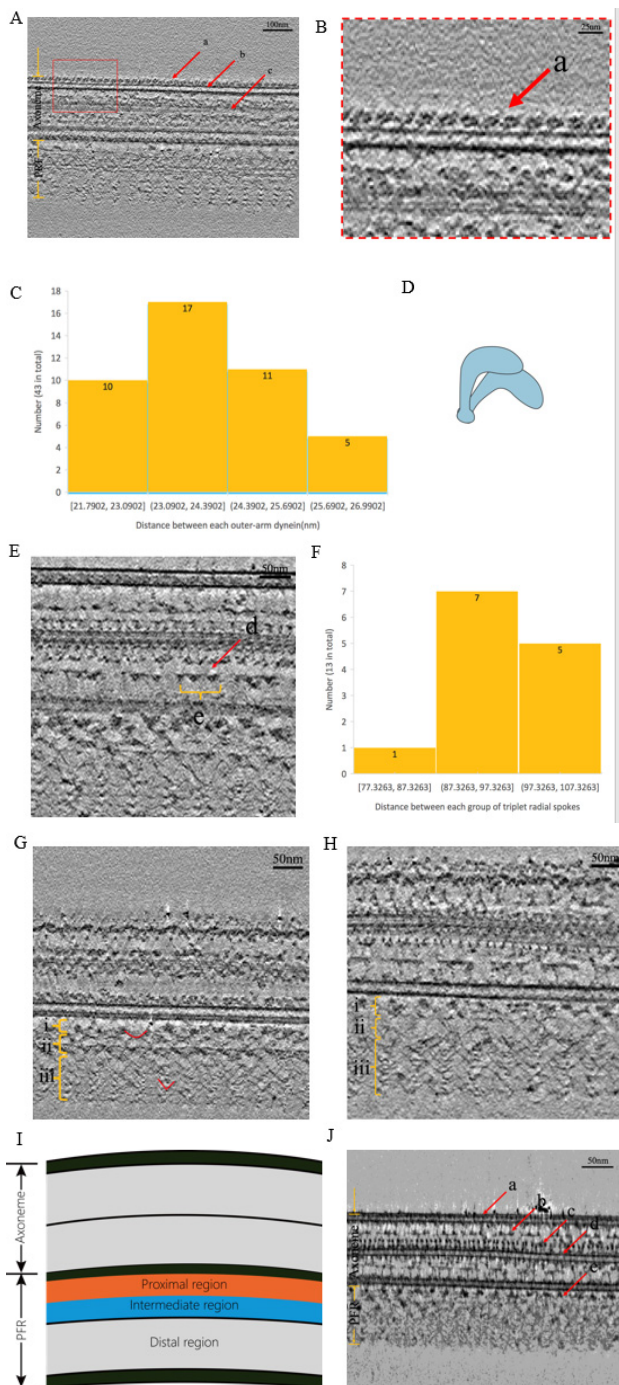


Figure 4. Longitudinal view of *T. brucei* axoneme.

(A) Image generated by the back-projection algorithm using the IMOD software. In this figure, the degree of x, y, z rotation is 0, 90, and 90, and view axis position is 37. The labels correspond to: a, outer-arm dynein; b, outer doublet microtubules; c, central pair apparatus.

(B) Detail of the outer-arm dynein structure indicated in (A) by the red box. The image reveals four outer-arm dyneins spaced approximately 96 nm apart.

(C) Figure illustrating the measurement of the distance between each outer-arm dynein; a total of 43 data were collected.

(D) The detailed structure of single outer-arm dynein shown in (B). Outer-arm dynein consists of two lobes of dynein with a thick head and a thin tail.

(E) Image generated by the back-projection algorithm using the IMOD software. The degree of x, y, z rotation in this figure is 0, 90 and 90, and the view axis position is 56. The labels correspond to: d, single radial spoke; b, triple radial spokes. Distance between each triple radial spoke is approximately 96 nm.

(F) Illustration of the measurement of the distance between the center of each group of triple radial spokes.

(G) Image generated by the back-projection algorithm using the IMOD software. The degree of x, y, z rotation in this figure is 0, 90, and 90, and the view axis position is 69. The labels correspond to: i, proximal domain; ii, intermediate domain; iii, distal domain. Detail of the PFR structure indicated in red line, which shows proximal domain has a wavy structure, while the structure of the distal domain resembles a mesh.

(H) Image generated by the back-projection algorithm using the IMOD software. The degree of x, y, z rotation in this figure is 0, 90, and 90, and the view axis position is 45. The labels correspond to: i, proximal domain; ii, intermediate domain; iii, distal domain.

(I) Approximate proportion of PFR in a flagellum of *T. brucei*.

(J) Image generated by the SIRT algorithm using the IMOD software. The degree of x, y, z rotation of this figure is 0, 90 and 90, and the view axis position is 69. The labels correspond to: a, outer doublet microtubules; b, radial spoke; c, central sheath; d, central pair apparatus; e, axoneme-PFR connectors.

4 Discussion

From the transection of *T. brucei* axoneme, a typical 9+2 arrangement is clearly observed. Axoneme consists of nine outer doublet microtubules, a central pair apparatus, outer-arm dyneins, inner-arm dyneins, NDRC and radial spokes. Each outer double microtubule consists of a complete A-tubule and a not completely circular B-tubule.

Dyneins are anchored on outer doublet microtubules. It relies on ATP to generate power and driving force for the movement of the flagellum. The dynein motor unit is highly complex, as it consists of one to three catalytic heavy chains (HC) and several associated light chains (LC), intermediate chains (IC), and light intermediate chains (LIC) [15]. It is well-recognized that flagellum motility is essential for the pathogenesis of *T. brucei*, however, little is known about the contribution of individual motility proteins. Future studies will identify the relationship among the subunits of outer-arm dynein by analyzing the impact of the knockout of specific subunits by RNAi methodology on virulence, vigor, and structure of *T. brucei*. Specifically, knockdown of the subunit of outer-arm dynein resulting in the change in the basal body pulsation will be indicative of its ability to control beat direction.

Each central pair apparatus originates from the basal plate and is connected to the outer doublet microtubules

via radial spokes. Radial spokes provide a platform for the assembly of signaling proteins [16,17]. In contrast to several other organisms, the central pair apparatus is relatively fixed for outer doublet microtubules in *T. brucei*, and is essential for *T. brucei* movement [18]. Thus, RNAi knockdown of protein components of the central pair apparatus results in severe motor deficits. In view of this result, future studies of drugs targeting the proteins of the central pair apparatus are warranted. Experiments with RNAi-mediated knockout demonstrate that deletion of different axoneme components, including dynamic protein motors, radial spokes, NDRC, and tubulin, all affect the normal motion of *T. brucei*.

Cross-section of *T. brucei* shows that the PFR has three distinct domains, i.e., proximal, intermediate, and distal domain. The current study demonstrated that the three domains have different structural features and dimensions. The proximal domain is wavy, while the distal domain has a mesh-like structure. In previous study, PFR has been documented to consist of PFR1 and PFR2 proteins, which not only provides structural support for the axoneme but also serve as a scaffold for the attachment of regulatory and functional proteins [19,20]. Given that the PFR is not present in the human host, it should be used as a critical therapeutic target in future studies. Thus, a significant amount of researches on the macromolecular organization of the PFR are still needed.

The trypanosome motility is characterized by its ability to cross the blood-brain barrier, which is the hallmark of the lethal phase of sleeping sickness. However, the treated drug does not cross the blood-brain barrier, causing the trypanosome to remain after treatment. *Brucei's* ability to cross the blood-brain barrier may be due to its helical motion that promotes tissue penetration. This led to a speculation if we could modify the gene of trypanosomes to make it as a carrier that carries drugs into the blood-brain barrier without harming the human host.

5 Conclusion

By using cryo-ET, we revealed the internal structure of axoneme and PFR, including outer doublet microtubules, central pair apparatus, dyneins, NDRC and radial spokes. Furthermore, we have identified the double-head structure of outer-arm dynein, 96 nm repeating unit, which arranged lengthwise in the model structure of an axoneme and internal structure of three domains of PFR.

These structures play a vital role in determining the pathogenicity of *Trypanosoma brucei*, thus resolving their internal organization would help us to find the treatments against African trypanosomiasis.

References

1. Simpson, A. G., Stevens, J. R. & Lukes, J. The evolution and diversity of kinetoplastid flagellates. *Trends Parasitol.* 22, 168–174 (2006).
2. Simarro P P , Jannin J , Cattand P . Eliminating human African trypanosomiasis: where do we stand

- and what comes next? [J]. *Plos Medicine*, 2008, 5(2):e55.
3. MacGregor, P., Savill, N. J., Hall, D. & Matthews, K. R. Transmission stages dominate trypanosome within- host dynamics during chronic infections. *Cell Host Microbe* 9, 310–318 (2011).
4. Hill, K. L. Mechanism and biology of trypanosome cell motility. *Eukaryot. Cell* 2, 200–208 (2003).
5. Frevert, U. et al. Early invasion of brain parenchyma by African trypanosomes. *PLoS ONE* 7, e43913 (2012).
6. Kennedy, P. G. Clinical features, diagnosis, and treatment of human African trypanosomiasis (sleeping sickness). *Lancet Neurol.* 12, 186–194 (2013).
7. Jamonneau, V. et al. Untreated human infections by *Trypanosoma brucei gambiense* are not 100% fatal. *PLoS Negl. Trop. Dis.* 6, e1691 (2012).
8. Simarro, P. P., Jannin, J. & Cattand, P. Eliminating human African trypanosomiasis: where do we stand and what comes next? *PLoS Med.* 5, e55 (2008).
9. Ralston, K. S., Kabututu, Z. P., Melehani, J. H., Oberholzer, M. & Hill, K. L. The *Trypanosoma brucei* flagellum: moving parasites in new directions. *Annu. Rev. Microbiol.* 63, 335–362 (2009).
10. Langousis G , Hill K L . Motility and more: the flagellum of *Trypanosoma brucei*[J]. *Nature Reviews Microbiology*, 2014, 12(7):505-518.
11. Kremer JR, Mastronarde DN, McIntosh JR (1996) Computer visualization of three- dimensional image data using IMOD. *J Struct Biol* 116:71–76.
12. IMOD User's Guide for Version 4.9: <http://bio3d.colorado.edu/imod/doc/guide.html>
13. Ralston K S , Kabututu Z P , Melehani J H , et al. The *Trypanosoma brucei* flagellum: moving parasites in new directions. [J]. *Annual Review of Microbiology*, 2009, 63(1):335-362.
14. Höög J L , Cédric Bouchet-Marquis, McIntosh J R , et al. Cryo-electron tomography and 3-D analysis of the intact flagellum in *Trypanosoma brucei*[J]. *Journal of Structural Biology*, 2012, 178(2):0-198.
15. King SM. Organization and regulation of the dynein microtubule motor. *Cell Biol Int.* 2003; 27:213–15. [PubMed: 12681312]
16. Smith EF, Yang P. The radial spokes and central apparatus: mechano-chemical transducers that regulate flagellar motility. *Cell Motil Cytoskelet.* 2004; 57:8–17.
17. Yang P, Diener DR, Yang C, Kohno T, Pazour GJ, et al. Radial spoke proteins of *Chlamydomonas* flagella. *J Cell Sci.* 2006; 119:1165–74. [PubMed: 16507594]
18. Mitchell DR, Nakatsugawa M. Bend propagation drives central pair rotation in *Chlamydomonas reinhardtii* flagella. *J Cell Biol.* 2004; 166:709–15. [PubMed: 15337779]

19. Ginger ML, Ngazoa ES, Pereira CA, Pullen TJ, Kabiri M, et al. Intracellular positioning of isoforms explains an unusually large adenylate kinase gene family in the parasite *Trypanosoma brucei*. *J Biol Chem.* 2005; 280:11781–89. [PubMed: 15657034]
20. Maga JA, LeBowitz JH. Unraveling the kinetoplastid paraflagellar rod. *Trends Cell Biol.* 1999; 9:409–13. [PubMed: 10481179]